An assessment of the Domain Reduction Method as an advanced boundary condition and some pitfalls in the use of conventional absorbing boundaries

ABSTRACT: This paper assesses the performance of two commonly used absorbing boundaries in dynamic finite element analysis of geotechnical problems in conjunction with the domain reduction method (DRM). The DRM was originally developed by Bielak et al [1] to reduce the computational cost of seismological applications, while Yoshimura et al [2] showed that it can be effectively used as a boundary condition. In the present study a practical methodology is proposed which employs the cone boundary of Kellezi [3] on the outer boundary of the reduced (step II) model of the DRM. To verify the applicability of the proposed methodology, the results using both the cone boundary and the standard viscous boundary are compared with those using an extended mesh. Finally results using the DRM as a boundary condition are compared with those using conventional boundary conditions. Some common pitfalls in the use of absorbing boundaries are highlighted and guidance for their correct use in engineering practice is given.

1 Introduction

One of the major issues in dynamic finite element analyses of soil-structure interaction (SSI) problems is to model accurately and economically the far-field medium. The most common way is to restrict the theoretically infinite computational domain to a finite one with artificial boundaries. The reduction of the solution domain makes the computation feasible, but spurious reflections from the artificial boundaries can seriously affect the accuracy of the results. Numerous artificial boundaries have been proposed in the literature over the last 30 years, which can be broadly categorized into three major groups [4]: elementary, local and consistent. Elementary boundaries are the ones commonly used for static analyses (i.e. zero stress or zero displacement boundary conditions) and they thus cannot model the geometric spreading of energy towards infinity. However, they are efficient in cases where the radiation damping is not important, like soft soil – stiff rock interfaces. On the other hand, consistent boundaries (e.g. Lysmer and Waas [5] and Kausel [6]) have mathematically complex formulations and satisfy exactly the radiation condition at the artificial boundary. However they are rarely used in practice as they are computationally expensive, frequency dependent and their implementation in finite element codes is often problematic. Finally in the case of local boundaries, the radiation condition is satisfied approximately at the artificial boundary, as the solution is local[1] in space and time. Local absorbing boundary conditions are widely used in

[1] When a formulation is local (as opposed to a global formulation) in space and time, the solution at a

practice as they provide results in most cases of acceptable accuracy and are far less computationally expensive than the more rigorous consistent boundaries. While numerous boundary conditions have been proposed in the literature (e.g. Clayton and Engquist [7], Enqguist and Majda [8], Barry et al [9], Komatitsch and Tromp [10], etc), the standard viscous boundary of Lysmer and Kuhlemeyer [11] remains the most widely used one. Detailed reviews of the various boundary conditions can be found in Kausel and Tassoulas [4], Givoli [12], Tsykov [13] and Kontoe [14].

The present study assesses the performance of simple absorbing boundary conditions (i.e. local boundaries) when they are used in conjunction with the Domain Reduction Method (DRM). The DRM was originally developed for seismological applications by Bielak *et al* [1]. It is a two-steps sub-structuring procedure that aims at reducing the domain that has to be modelled numerically by a change of governing variables. The DRM has been implemented in the finite element code ICFEP (Potts & Zdravković [15] and further developed to deal with dynamic coupled consolidation problems (Kontoe [14]; Kontoe *et al* [16]). Figure 1 summarizes the two steps of the DRM. In the first step of the DRM, a simplified background model is analysed that

---

specific boundary degree of freedom depends on the response of only adjacent boundary degrees of freedom at a specific time, or at most, during a limited past period.

includes the source of excitation and the wave propagation path in a half-space, but only a crude representation of the area of interest (that contains localised geological features or geotechnical structures). Since structures or geological features of short wavelengths are eliminated from the background model, the computation cost of the step I analysis is very small compared to the cost of analysing the complete domain (Figure 1a), as larger elements can be used. The second step is performed on a reduced domain (Figure 1b) that comprises of the area of interest Ω and of a small external region $\hat{\Omega}^+$. The seismic excitation is directly introduced into the computational domain, in the form of equivalent forces (and fluid flows if a coupled consolidation analysis is performed) calculated in the first step. Hence the effective nodal forces ΔP^{eff} (and fluid flows), calculated from the incremental displacements, velocities and accelerations computed in step I, are applied to the model of step II in the elements located within the boundaries Γ_e and Γ. The perturbation in the external area $\hat{\Omega}^+$ is only outgoing and corresponds to the deviation of the area of interest from the background model.

Cremonini *et al* [17] used an earlier version of the DRM to show that this sub-structuring technique can be successfully used in conjunction with local absorbing boundary conditions. Yoshimura *et al* [2] showed the applicability of the DRM in large scale three dimensional domains containing the causative fault and strong geological and topographical irregularities (e.g. sedimentary basins). Based on the results of their case study, they concluded that the method improves the performance of conventional boundary conditions like the standard viscous boundary of Lysmer and Kuhlemeyer [11]. Yoshimura *et al* [2] suggested that since the perturbation in the external area $\hat{\Omega}^+$ corresponds only to the deviation of the area of interest from the

background model, the absorbing boundaries are required to absorb less energy and they therefore perform better. Assimaki et al [18] used a similar sub-structuring methodology to examine topographic effects on the seismic ground motion. In their model they prescribe the input motion in the form of effective forcing functions and they employ absorbing elements around the discretized domain.

The aim of the present study is to show in a systematic way that the DRM, in conjunction with a conventional absorbing boundary (i.e. the standard viscous boundary of Lysmer and Kuhlemeyer [11]), can be efficiently used in the numerical modelling of geotechnical earthquake engineering problems as an advanced absorbing boundary condition. In this respect, a practical methodology is also proposed which employs the cone boundary of Kellezi [3] on the outer boundary of the reduced (step II) model of the DRM. To verify the applicability of the proposed methodology, the results using the cone boundary and the viscous boundary are compared with those using an extended mesh. The second part of the papers compares results using the DRM as a boundary condition with those obtained using conventional boundary conditions. Particular emphasis is placed on identifying common pitfalls in the use of conventional absorbing boundaries in engineering practice that can lead in erroneous results.

2 Methodology

As noted earlier, the DRM has a dual role as it not only reduces the domain that has to be modelled numerically, but in conjunction with an absorbing boundary it serves as an advanced boundary condition. In particular, numerical examples by

Yoshimura *et al* [2] showed that the ground motion in the external area $\hat{\Omega}^+$ is generally small compared to the motion in the area Ω^+ of the free-field model. Hence the absorbing boundaries perform better when incorporated in the DRM, as they are required to absorb less energy. In the present study the widely used standard viscous boundary of Lysmer and Kuhlemeyer [11] and the cone boundary of Kellezi [3] were incorporated in the DRM.

In two dimensions the mechanical equivalent of the standard viscous boundary is a system of two series of infinitesimal dashpots (which are integrated to give discrete nodal springs) oriented normal and tangential to the boundary of the mesh (Figure 2a), defined by:

$$\sigma = \rho V_P \dot{u} \qquad (1)$$

$$\tau = \rho V_s \dot{v} \qquad (2)$$

where $\dot{u}$, $\dot{v}$, σ and τ are the normal and the tangential velocities and stresses respectively, ρ is the mass density of the soil and V_P,V_S are the velocities of the P-waves and S-waves respectively. In addition to the viscous dashpots, the cone boundary also consists of a series of infinitesimal springs oriented normal and tangential to the boundary of the mesh (Figure 2b). For plane strain analysis, the springs are defined by:

$$\sigma = \rho \frac{V_P^{\,2}}{2r} u \qquad (3)$$

$$\tau = \rho \frac{V_S^{\,2}}{2r} v \qquad (4)$$

where r is the distance from the boundary node to the source location and u, v are the normal and the tangential displacements respectively. Thanks to the spring term, the cone boundary approximates the stiffness of the unbounded soil domain and it eliminates the permanent movement that occurs if only the viscous boundary is preset at low frequencies. This shortcoming of the viscous boundary has been widely recognised (e.g. Cohen & Jennings [19], Simons & Randolph [20], Siller *et al* [21] and Kellezi [3]). The limitation however of the cone boundary is the fact that the spring stiffness is a function of the distance (r) of the boundary from the source of excitation. Consequently, to date, the cone boundary has only been employed in problems with surface excitations (e.g. dynamic pile loading, moving vehicles) where the distance of a boundary from the source is known. In seismic SSI problems the distance from the seismic source (fault) is difficult to be accurately determined. Furthermore, even in cases where the location of the fault is known, modelling of the fault is rarely undertaken because it results in excessively large computational domains. The seismic excitation is typically applied along the bottom mesh boundary. If this is applied at the boundary nodes in terms of accelerations, equivalent velocities or displacements no absorbing boundary condition can be specified at the bottom boundary together with the excitation due to the finite element node constraints imposed. Absorbing boundary conditions can be applied at the bottom of the mesh together with the excitation, only if the excitation is in the form of forcing functions that result to the target input motion (i.e. step I of the DRM), since in that case the response of the bottom boundary nodes is not constrained. In addition, the cone boundary cannot be used at the lateral boundaries of the mesh, since the concept of geometrical spreading towards infinity does not apply in this case (i.e. it is not possible to determine r, as the source of excitation occurs along a complete mesh

boundary). In this section, a practical methodology is proposed which employs the cone boundary on the outer boundary of the reduced (step II) model of the DRM.

According to the DRM formulation, waves reaching the outer boundary $\hat{\Gamma}^+$ of the reduced domain (i.e. step II model) are only due to the deviation of the area of interest from the background model (i.e. step I model). In cases where the only additional element of the reduced domain is a structure (e.g. tunnel, retaining wall), the perturbation in $\hat{\Omega}^+$ is only due to waves reflected from this structure. Therefore this structure can be considered as the "excitation source" for the external area $\hat{\Omega}^+$. The idea is to calculate the stiffness terms of the cone boundary based on the distance of the structure from the boundary. Since the structure is not a point source and has finite dimensions, the theoretical value of the distance r for each boundary node needs to be approximated. Figure 3 illustrates a step II model of the DRM containing a structure ABCD. If the structure is considered as the "excitation source" for the area $\hat{\Omega}^+$, the r of each boundary node can be approximated as the distance to the closest point of the structure. For example, along the boundary A_1A_2 r is the distance from the point A, along the boundary A_2B_1 r is constant equal to $\overline{A_2A}$ and along the boundary B_1B_3 r is the distance from the point B. In a similar way, the distance r can be calculated for the rest of the boundary nodes of $\hat{\Gamma}^+$. Numerical tests by Kellezi [22] and by Kontoe [14] show that the performance of the cone boundary is relatively insensitive to the dashpot and spring coefficients. Therefore, one would expect that the preceding approximation of r is sufficient.

3 Numerical results and discussions

In this section the proposed methodology is tested in a dynamic analysis of a cut and cover tunnel. Hence to verify the applicability of the cone boundary to the DRM, the reduced model of Figure 4 was used for the step II calculations. Prior to the dynamic analysis, a static analysis was undertaken to model the tunnel construction sequence. During the static analysis horizontal displacements were restricted along the outer boundary $\hat{\Gamma}^{+}$ while vertical displacements were restricted along the bottom mesh boundary. Initially, the side walls of the tunnel were constructed as wished in place and the excavation was then performed in ten stages. During the excavation (i.e. of the elements originally occupying the tunnel), the walls were supported by restricting their horizontal movement. Subsequently, the bottom and the top slabs were constructed, the horizontal support to the wall was removed (i.e. the prescribed horizontal displacements were released) and the area above the top slab was backfilled with soil. In all analyses linear elastic drained soil behaviour was assumed. Equations 3 and 4 were used to calculate the springs' stresses, treating the tunnel as the source of excitation, according to the procedure described in the previous section. Furthermore all step II analyses were repeated with the viscous boundary.

One of the advantages of the DRM is that one can achieve significant savings in the computational cost using a 1-D Finite Element column (extending down to the bedrock) as a background model in the step I analysis to calculate the free-field response. To demonstrate this feature of the DRM, a 1-D model of a soil column 4m wide and 612m deep was considered for the background analysis (i.e. step I). The column consists of 408 (2x204) 8-noded elements. Vertical displacements were restricted along the bottom and the side boundaries. The background analysis was

repeated for three acceleration sinusoidal pulses of periods T_o =1sec, 2sec and 4sec. The excitations with amplitude of 1m/sec^2 were applied incrementally, with a time step equal to T_o/20, in the horizontal direction along the bottom boundary. The investigation time is only 6sec and the 1-D extended mesh is taken deep enough to prevent reflections from the bottom boundary to the area of interest. Although only the case of vertical incidence of the incoming seismic waves was considered in the present study, the DRM is generally applicable to arbitrary seismic excitation.

In all the analyses, the time integration was performed with the Generalised-α method (Chung and Hulbert [23], Kontoe *et al* [24]) and both the soil and the cut and cover tunnel were modelled as linear elastic materials, with the material properties listed in Table 1. It should be noted that no material damping was considered for the validation examples.

To validate the applicability of the cone boundary, the step II analyses were also repeated with an extended mesh 933m wide and 466m deep. This model is taken big enough to prevent reflections from the boundary to the area of interest. Along the boundary $\hat{\Gamma}^+$ of the extended mesh displacements were restricted in both directions. The validation model consists of 29522 8-noded elements and has the same element dimensions as the reduced model of Figure 4.

During the step I analyses the incremental displacements were calculated at various depths of the 1-D model. These were then used in the step II analyses to calculate the equivalent forces which were applied to the corresponding nodes of the step II models, located between the boundaries Γ_e and Γ. It should also be highlighted that this verification example subjects the absorbing boundaries to severe test

conditions. It is widely accepted that the performance of local absorbing boundaries is more accurate for high frequencies (see for example Enqguist and Majda [8], Barry et al [9], Kellezi [22], Kontoe [14], etc). Therefore the selected low frequency excitation pulses challenge the limits of their capabilities. Furthermore, Kellezi [22] suggests that the absorbing boundary should not be placed closer than (1.2-1.5)λ_S from the excitation source, where λ_S is the wavelength of the SV-wave corresponding to the predominant period of the excitation. Considering the suggestion of Kellezi [22], it becomes clear that the absorbing boundaries have been placed very close (0.2 λ_S -0.7 λ_S) to the tunnel, which in this case is the assumed "source" of excitation.

The response was monitored at the surface node C (50.0, 0.0) and at node D (60.0, -60.0) (Figure 4). It should be noted that these nodes lie in the internal area Ω, and they therefore record the total response (free-field response plus reflections from the structure). Figures 5-7 compare the predicted displacements of the three models (cone boundary, viscous boundary and extended mesh) for pulses of 3 periods (T_o = 1.0s, 2.0s and 4.0s).

Since the loading is applied only in the horizontal direction, the horizontal response is dominant. However, due to multiple reflections from the tunnel, vertical displacements are also recorded at both nodes. Regarding the horizontal displacements, the results of both absorbing boundaries (cone, viscous) compare near perfectly with the ones of the extended mesh, irrespective of the period of the loading.

On the other hand, the accuracy of the vertical response predicted by both absorbing boundaries deteriorates as the period of the loading increases. However, considering that this numerical test is quite challenging for both absorbing boundaries,

it can be said that their performance is unexpectedly good. This can be attributed to their application in the external area of the DRM model, where they are required to absorb less energy. Comparing the viscous boundary with the cone boundary, it is clear that the cone boundary performs better for all periods.

Figure 8 shows the vertical acceleration response at nodes C, D for pulses of 2 periods (T_o = 2.0s and 4.0s). Both absorbing boundaries seem to give more accurate results in terms of vertical accelerations than in terms of vertical displacements. This is not surprising, as the acceleration response is dominated by the higher frequencies of the system. Figure 9 shows the displacement response at node G (82.0, -82.0) (see Figure 4), which is located very close to the outer boundary $\hat{\Gamma}^+$, for pulses of 2 periods (T_o = 2.0s and 4.0s). The response recorded at node G is purely due to reflections from the structure. Hence, the horizontal displacements are much smaller than the ones recorded at nodes C, D, whereas the vertical displacements are of the same order of magnitude. The errors associated with both absorbing boundaries are larger in the plots of horizontal displacements. The vertical displacements predicted by the cone boundary are however more accurate than those predicted by the viscous boundary. For example in Figure 9b the error in predicting the maximum response of the viscous boundary is 62% at t=3.8s, while the corresponding error of the cone boundary is 16%.

Figure 10 plots the vertical displacement response recorded at nodes Q (13.0, -1.0), R (15.0, -2.0) of the structure and the corresponding axial force time histories at integration points Q'(13.5, -1.0) and R' (15.0, -2.5) computed by the three models for T=4.0s. The structural response reveals that the two absorbing boundaries compare very well with the extended mesh both in terms of displacements and axial forces.

However, the viscous boundary is consistently slightly less accurate than the cone boundary. For example in Figure 10a the viscous boundary under predicts the maximum displacement by 7.0%, while the corresponding error for the cone boundary is 0.5%.

Overall, the validation examples have shown that the cone boundary can be used in the reduced model of the DRM. It has also been observed that the ability of both absorbing boundaries to absorb reflected waves is very similar, although the cone boundary seems to give slightly more accurate results.

In the preceding example the excitation was a simple pulse and the investigation time was limited to avoid reflections from the Dirichlet boundaries of the extended model. In order to compare the performance of the two absorbing boundaries in a more realistic scenario, the previous analysis was repeated with an earthquake excitation. The UNAM acceleration time history, recorded during the 1985 Mexico earthquake, was the input motion for the step I analysis. The 1-D background model was subjected to 60 seconds of the filtered recording with a time step of 0.01 sec (Figure 11a). A fourth order band-pass Butterworth filter was used to remove the extreme low ($f<0.1$Hz) and high frequency ($f>25$Hz) components of the record. The Mexico acceleration time history was specifically selected for its low frequency content (see Figure 11b).

Figure 12 shows the displacement response recorded at nodes C, D for both absorbing boundaries. As observed with the sinusoidal excitation results, both boundaries give near identical results in terms of horizontal displacements. Regarding the vertical displacements the viscous boundary predicts up to a 30% lower response

than the cone boundary. Furthermore, the two absorbing boundaries predict identical acceleration time histories, which are not included herein for brevity. As the system was subjected to a particularly low frequency excitation, one would expect considerable differences in the predicted responses of the two boundaries. This is not the case, due to the improved performance of the viscous boundary when used in the external area of the DRM model.

4 Comparison with a conventional method of analysis

One of the basic requirements in dynamic analyses of SSI problems is that the width of the mesh and the lateral boundary conditions are such that free-field conditions (i.e. one-dimensional soil response) occur near to the lateral boundaries of the mesh. As mentioned earlier, in conventional analyses the seismic excitation is typically applied as an acceleration time history along the bottom mesh boundary at the soil-rock interface. Furthermore, local boundaries are usually applied along the lateral sides of the mesh. The major limitation of this approach is that free-field conditions are very difficult to recover along the lateral sides of the mesh. There are numerous examples of dynamic SSI analyses in the literature where such a configuration is adopted: analyses of piles [25, 26], retaining walls [27, 28], tunnels [29] etc.

In this section the ability of the DRM as a boundary condition to attain free-field conditions at the lateral sides of the mesh is compared with that of conventional analysis. The numerical model of Figure 4 was employed for the conventional analysis, applying the standard viscous boundary along the lateral sides of the mesh.

The DRM model (denoted as DRM+SVB in future discussions) was compared with the conventional one (denoted as SVB in future discussions) for two sets of analyses. The seismic excitation in the first set of analyses was the north-south KJMA acceleration time history, recorded during the 1995 Kobe earthquake, while for the second set of analyses the north-south Veliki acceleration time history, recorded during the 1978 Montenegro earthquake, was used. Figure 13 shows the normalised, with respect to the peak ground acceleration, acceleration response spectra of the two excitations. In both sets of analyses, the acceleration time history was applied incrementally in the horizontal direction along the base of the mesh, while the corresponding vertical displacements were restricted. For the step I DRM analysis a 1-D model of a soil column 2m wide and 86m deep, consisting of 172 8-noded elements, was considered. Vertical displacements were restricted along the bottom and the side boundaries. To allow comparison with the conventional analysis the numerical model of Figure 4 was also employed in the step II DRM analysis. The standard viscous boundary was applied along the lateral sides of the mesh, while horizontal and vertical displacements were restricted along the bottom boundary. Prior to the dynamic analyses, the construction sequence was simulated to establish the initial stress state as described in the previous section. In all analyses 2% Rayleigh damping was employed. The values of the Rayleigh damping coefficients (A and B) are listed in Table 1.

As the main focus of this section is to compare the ability of the two boundary conditions to simulate the free-field response in the far field, i.e. at some distance away from the structure, the response at various distances from the axis of symmetry of the 2D FE models (see Figure 4), is compared with the one computed

with the 1D model. Hence, Figure 14 plots the loci of maximum horizontal displacement with depth computed with the DRM+SVB model (at x=58.0), the SVB model (at x=58.0 and 78.0m) and the 1D model. The DRM+SVB response compares very well with the 1D one for both excitations. Thus the free-field conditions seem to be attained at x=58.0m. Note that the two points for z=-68.0 and -78.0m of the DRM+SVB model have not been plotted as they refer to the external area of the DRM, where only the relative response to the free field one is computed. On the other hand the SVB model response significantly differs from the 1D one for both excitations. The inability of the SVB model to reproduce free-field conditions appears to be more pronounced for the KJMA excitation than for the Veliki one. As previously discussed it is widely accepted that the performance of local absorbing boundaries is less accurate for low frequencies. Therefore the difference in the performance of the SVB for the two excitations could be attributed to the richer frequency content of the KJMA in the low frequency range (i.e. T>0.5s in Figure 13). Furthermore, one would expect the predicted response by the SVB model to match the 1D response for large distances from the axis of symmetry. On the contrary, it is interesting to note that the greater is the distance from the axis of symmetry the lower is the SVB response.

Figures 15 and 16 compare the horizontal displacement time histories recorded at node T (see Figure 4) of the DRM+SVB and SVB models with the corresponding ones of the 1D model for the KJMA and Veliki excitations respectively. The curves for the DRM+SVB and 1D models are indistinguishable for both excitations, verifying the ability of the DRM+SVB model to reproduce free-field conditions away from the structure. Conversely the predicted response by the SVB

model is significantly different from the 1D situation both in terms of amplitude and frequency content. These differences are again more pronounced for the KJMA excitation. Since the main objective of a SSI analysis is the realistic modelling of the structural response, Figure 17 compares the axial force, bending moment and shear force time histories computed by the DRM+SVB and SVB models monitored at the integration point Q' (13.5, -1.0) of the structure. Significant differences can be observed in the plots of axial force, bending moment and shear force time histories. The differences in terms of the maximum predicted value are 6%, 28% and 29% for the axial force, bending moment and shear force time histories respectively.

The inability of the SVB model to reproduce the 1D free-field response at the side boundaries of the mesh seems to significantly affect the structural response and it can be attributed to the poor performance of the viscous dashpots. It is widely known that the viscous boundary is exact for perpendicularly impinging waves. Furthermore, for both 2D and 3D cases, optimal absorption is achieved for angles of incidence greater than 30° (when the angle is measured from the direction parallel to the boundary). At large distances from the excitation source the waves propagate one-dimensionally in approximately the direction of the normal to the artificial boundary. Consequently, the performance of the viscous boundary improves significantly the farther it is placed away from the source of excitation. In the 2D model of Figure 4, the dashpots were placed very close to the seismic excitation (which was applied along the bottom boundary of the mesh), especially at the bottom corners of the mesh, and the shear waves propagate in a direction parallel to the viscous boundary. To further investigate this, analyses were carried out with wider meshes. The two sets of analyses (i.e. for the Veliki and KJMA records) were initially repeated with a mesh of

total width of 204.0m. Figure 18 compares the loci of maximum horizontal displacement with depth computed by the DRM+SVB (at x=58.0) and the SVB (at x=58.0, 78.0 and 98.0m) models using the 204x86m mesh, with the one obtained by the 1D model. Comparing Figures 14 and 18, it can be observed that the DRM+SVB model is insensitive to the width of the mesh, predicting very well the free-field response for both meshes and excitations. Conversely the performance of the SVB model appears to be mesh dependent, tending to improve as the width of the mesh increases. The improvement of the SVB performance is more noticeable for the Veliki record, while for the KJMA it still severely over-damps the response. Hence, once more, the accuracy of the SVB model seems to depend on the frequency content of the excitation. Therefore when using the SVB configuration the same mesh width cannot be necessarily used for excitations of different frequency content. To further investigate the sensitivity of the SVB model to the width of the mesh, the analyses for the KJMA record were repeated using a mesh of total width of 300.0m. Some indicative results from these analyses are presented in Figure 19. Clearly the SVB model, even when a 300m wide mesh is used, still under-predicts the free-field response. Comparing Figures 15b and 19b it becomes evident that when a large mesh is used the SVB response is more comparable with the 1D one, especially for the first 10sec of the earthquake. However, in order to get acceptable representation of the free-field response for the KJMA record with the SVB model, one should clearly use an even wider mesh.

Table 2 summarizes the computational cost of all the analyses. The computational cost of the DRM+SVB model is no more than 2.3% higher than the cost of the SVB model for all the analyses. However it was shown that when using the

DRM method one can use a very small mesh, while the SVB model requires the use of a significantly wider mesh (actually an even larger mesh is needed to obtain similar accuracy as explained above). Therefore for the KJMA excitation the computational cost of the SVB model is at least 30% higher than the one of the DRM+SVB model. Acceptable accuracy would be achieved with the conventional configuration only using uneconomically large meshes. This demonstrates the superiority of the DRM solution, as it gives accurate predictions using a significantly smaller model than conventional methods.

It has also been demonstrated that the poor performance of the SVB model can be attributed to the misuse of the viscous boundary. The excellent performance of the viscous dashpots in the DRM+SVB model verifies this speculation. In the DRM simulation the excitation was introduced into the mesh and the motion in area $\hat{\Omega}^+$ (see Figure 4) was only outgoing, due to reflections from the structure. Hence in the DRM+SVB model the viscous boundary performed well because it was placed away from the excitation and had to absorb less energy.

5 Conclusions

The great advantage of the DRM is that the excitation is directly introduced into the computational domain, leaving more flexibility in the choice of appropriate boundary conditions. Hence, a methodology has been suggested which employs the cone boundary on the external boundary $\hat{\Gamma}^+$ of the reduced domain. A cut and cover tunnel was analysed with both the cone and the viscous boundary. To verify the applicability of the cone boundary, the step II analyses were repeated with an

extended mesh. The cone boundary was found to be slightly superior to the viscous boundary. Both boundaries were subjected to a challenging numerical test and they both performed very well.

Furthermore the ability of the DRM as a boundary condition to attain free-field conditions near the far boundaries of the mesh was compared with that of conventional analysis. For the conventional model a widely used configuration was employed: the excitation was applied at the bottom of the mesh, while the standard viscous boundary was applied along the two lateral sides. This arrangement failed to reproduce the free-field response and led to underestimation of both the soil and the structural response in the near field with respect to the DRM analysis. Furthermore, the conventional model was found to be very sensitive both to the mesh size and the frequency content of the excitation. The poor performance of the conventional model can be attributed to the fact that the dashpots were placed very close to the excitation (i.e. bottom boundary of the mesh). Conversely the viscous dashpots performed very well when they were used together with the DRM method. The DRM model essentially allowed the dashpots to be placed at some distance from the excitation as they only had to absorb the scattered energy from the structure.

Although all the above considerations where performed for a linear elastic system, the procedures are expected to be applicable to problems with nonlinear material behaviour (in the internal area of the DRM model). However the magnitude of any errors introduced due to the use of local boundaries with constant viscosity and stiffness values in the analysis needs to be further investigated.

6 References

1 Bielak J., Loukakis K., Hisada Y. & Yoshimura C. (2003), "Domain Reduction Method for Three-Dimensional Earthquake Modeling in Localized Regions, Part I: Theory", Bulletin of the Seismological Society of America, Vol. 93, No 2, pp. 817-824.

2 Yoshimura C., Bielak J., Hisada Y. & Fernández A. (2003), "Domain Reduction Method for Three-Dimensional Earthquake Modeling in Localized Regions, Part II: Verification and Applications", Bulletin of the Seismological Society of America, Vol. 93, No 2, pp. 825-840.

3 Kellezi L. (2000), "Local transmitting boundaries for transient elastic analysis", Soil Dynamics and Earthquake Engineering, Vol.19, pp. 533-547.

4 Kausel E. & Tassoulas J. L. (1981), "Transmitting Boundaries: A closed-form comparison", Bulletin of the Seismological Society of America, Vol. 71, No 1, pp.143-159.

5 Lysmer J. & Waas G. (1972), "Shear waves in plane infinite structures", Journal of Engineering Mechanics Division, ASCE Vol. 98, No. 1, pp.85-105.

6 Kausel E. (1994), "Thin-layer method: formulation in time domain", International Journal for Numerical Methods in Engineering, Vol.37, pp.927-941.

7 Clayton R.W. & Engquist B. (1977), "Absorbing boundary conditions for acoustic and elastic wave equation", Bulletin of the Seismological Society of America, Vol. 67, No 6, pp. 1529-1541.

8 Engquist, M. & Majda, A. (1977), “Absorbing boundary conditions for the numerical simulation of waves” Journal of Mathematics of Computation, Vol.31, No.139, pp.629-651.

9 Barry, A., Bielak J. & MacCamy, R.C. (1988), “On absorbing boundary conditions for wave propagation” Journal of Computational Physics, Vol. 79, No.2, pp.449-468.

10 Komatitsch, D. & Tromp J.(2003), “A perfectly matched layer absorbing boundary condition for the second-order seismic wave equation”, International Geophysical Journal, Vol. 154, No.1, 146–153.

11 Lysmer J. & Kuhlemeyer R.L. (1969), “Finite dynamic model for infinite media” Journal of the Engineering Mechanics Division, ASCE, Vol.95, No.4, pp. 859-877.

12 Givoli D., (1991) “Non-reflecting boundary conditions” Journal of Computational Physics, Vol. 94, No.1, pp.1-29.

13 Tsynkov, S.V. (1998), “Numerical solution of problems on unbounded domains. A review.”, Applied Numerical Mathematics, Vol.27,pp. 465-532.

14 Kontoe S. (2006), “Development of time integration schemes and advanced boundary conditions for dynamic geotechnical analysis”, PhD thesis, Imperial College, London.

15 Potts D.M. & Zdravković L.T. (1999), Finite element analysis in geotechnical engineering: theory, Thomas Telford, London.

16 Kontoe S., Zdravković L. & Potts D.M. (2007) "The Domain Reduction Method for dynamic coupled consolidation problems in geotechnical engineering" International Journal for Numerical and Analytical Methods in Geomechanics, in press, doi: 10.1002/nag.641.

17 Cremonini M.G. & Christiano P. & Bielak J. (1988), "Implementation of the effective seismic input for soil-structure interaction systems", *Earthquake Engineering & Structural Dynamics*, Vol. 16, pp. 615-625.

18 Assimaki, D., Gazetas, G. & Kausel, E. (2005), "Effects of local soil conditions on the topographic aggravation of seismic motion: parametric investigation and recorded field evidence from the 1999 Athens earthquake", BSSA, Vol.95, No.3, pp. 1059-1089.

19 Cohen M. & Jennings P.C. (1983), "Silent boundary methods for transient analysis" in Belytschko T. & Hughes T.J.R eds., *Computational Methods for transient analysis*, pp.301-360.

20 Simons, H.A. & Randolph, M.F. (1986), Short Communication, "Comparison of transmitting boundaries in dynamic finite element analyses using explicit time integration", *International Journal for Numerical and Analytical Methods in Geomechanics*, Vol.10, pp.329-342.

21 Siller, T.J., Christiano, P.P. & Bielak, J. (1991), " Seismic response of tied-back retaining walls", *Earthquake Engineering & Structural Dynamics*, Vol.20, pp.605-620.

22 Kellezi L. (1998), "Dynamic soil-structure interaction transmitting boundary for transient analysis", PhD Thesis, Department of Structural Engineering and Materials, Technical University of Denmark.

23 Chung J. & Hulbert, G.M. (1993), "A time integration algorithm for structural dynamics with improved numerical dissipation: the generalized-α method", Journal of Applied Mechanics, Vol. 60, pp. 371–375.

24 Kontoe S., Zdravković L. & Potts D.M. (2007) "An assessment of time integration schemes for dynamic geotechnical problems", Computers and Geotechnics, accepted, in press. doi:10.1016/j.compgeo.2007.05.001.

25 Brown D.A., O'Neill M.W., Hoit M., McVay M., El Naggar M.H. & Chakraborty S., (2001), "Static and Dynamic Lateral Loading of Pile Groups", NCHRP report 461, National Academy Press, Washington, D.C.

26 Maheshwari B.K., Truman K.Z., El Naggar M.H. & Gould P. L. (2004), "Three-dimensional finite element nonlinear dynamic analysis of pile groups for lateral transient and seismic excitations" Canadian Geotechnical Journal, Vol. 41, pp. 118-133.

27 Woodward P.K. & Griffiths D.V. (1996), "Comparison of pseudo-static and dynamic behaviour of gravity retaining walls", Geotechnical and Geological Engineering, Vol.14, pp. 269-290.

28 Tsopanakis Y., Psarropoulos P.N. & Tsimpourakis S. (2007), "Dynamic interaction between retaining walls and retained structures", Proceeding of the 4th

International Conference on earthquake Engineering, paper No1270, Thessaloniki, Greece.

29 Bilotta E., Lanzano G., Russo G., Santucci de Magistris F., Aiello V., Conte E., Silvestri F. & Valentino M. (2007), "Pseudotsatic and dynamic analyses of tunnels in transversal and longitudinal directions." Proceeding of the 4th International Conference on earthquake Engineering, paper No1550, Thessaloniki, Greece.

7 Appendix: Notation

E' Young's modulus.

u and v Displacement components.

r Distance from the boundary nodes to the source location.

V_P Compression wave velocity of propagation.

V_S Shear wave velocity of propagation.

γ Bulk unit weight of soil.

Γ Boundary between the internal (Ω) and the external area (Ω^+) in the domain reduction method.

Γ^+ Outer boundary of the external area (Ω^+) in the domain reduction method.

$\hat{\Gamma}$ Outer boundary of the external area ($\hat{\Omega}^+$) of the reduced model in the domain reduction method.

Γ_e Boundary within the external area of the background model in the domain reduction method defining a strip of elements between Γ_e and Γ.

Δt Incremental time step.

λ_S Wavelength of the SV-wave corresponding to the predominant period of the

excitation.

ν' Poisson's ratio.

ρ Material density.

σ, τ Normal and tangential stresses respectively.

Ω Internal area of both the reduced and the background models in the domain reduction method.

Ω^+ External area of both the reduced and the background models in the domain reduction method.

Ω^0 Internal area of the background model in the domain reduction method.

$\hat{\Omega}^+$ External area of the reduced model in the domain reduction method.

8 Figures

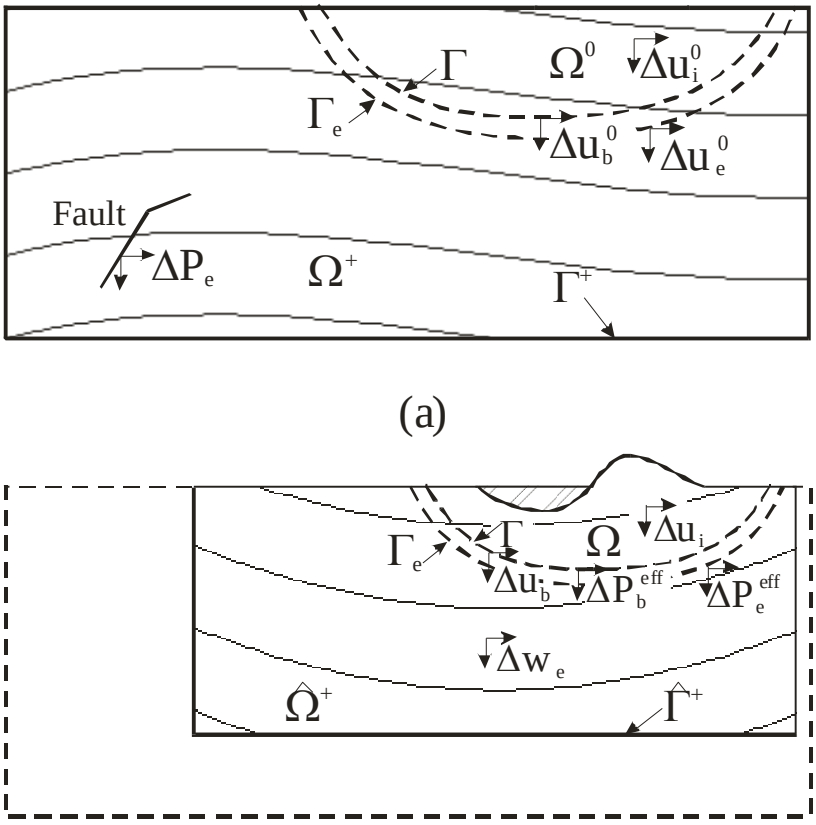

Figure 1: Summary of the two steps of DRM (after Bielak *et al* [13])

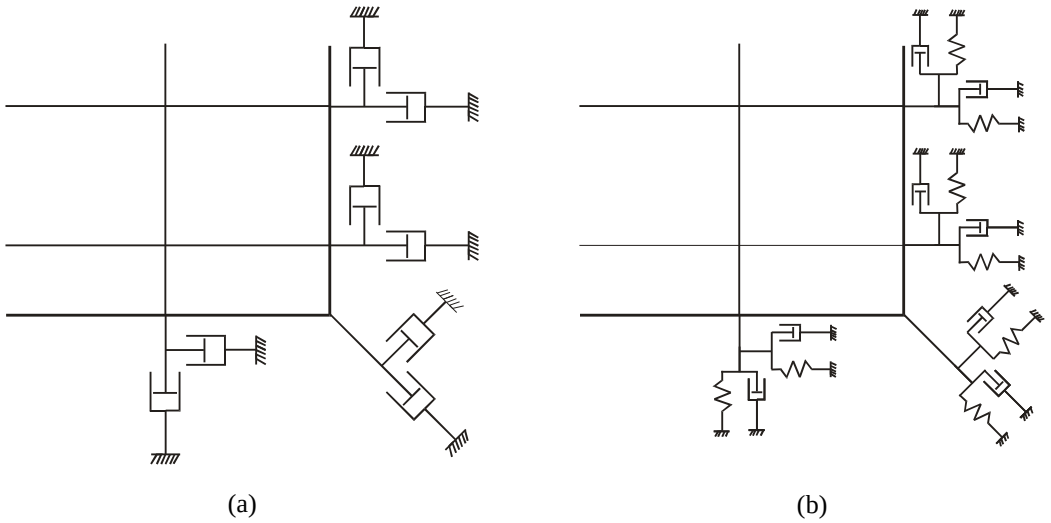

Figure 2: Mechanical representation of the standard viscous boundary (a) and the cone boundary (b).

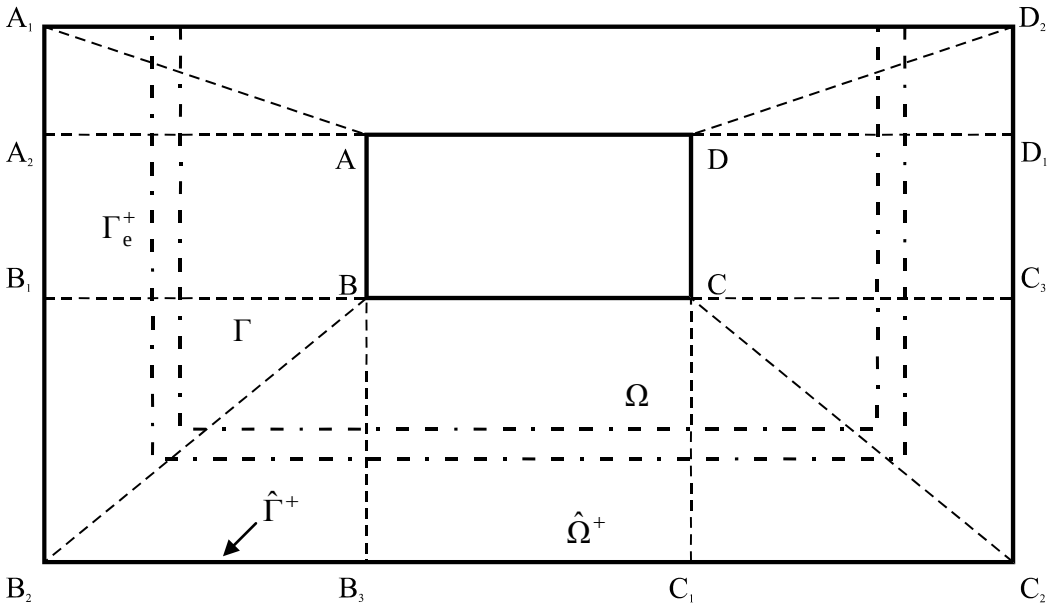

Figure3: Step II model of the DRM containing a structure ABCD

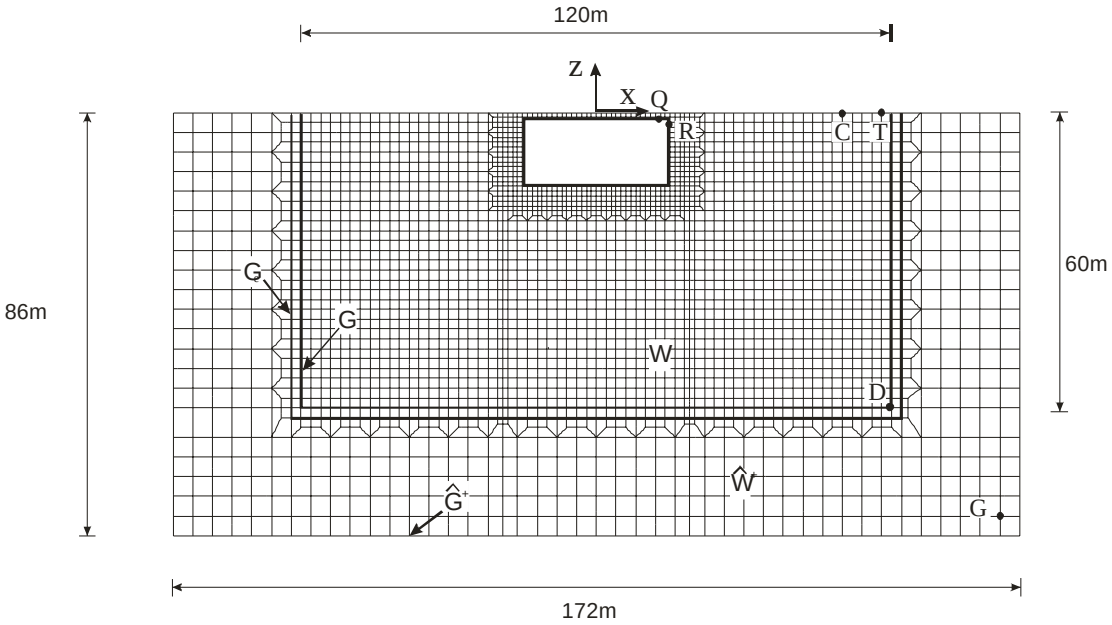

Figure 4: Mesh discretization.

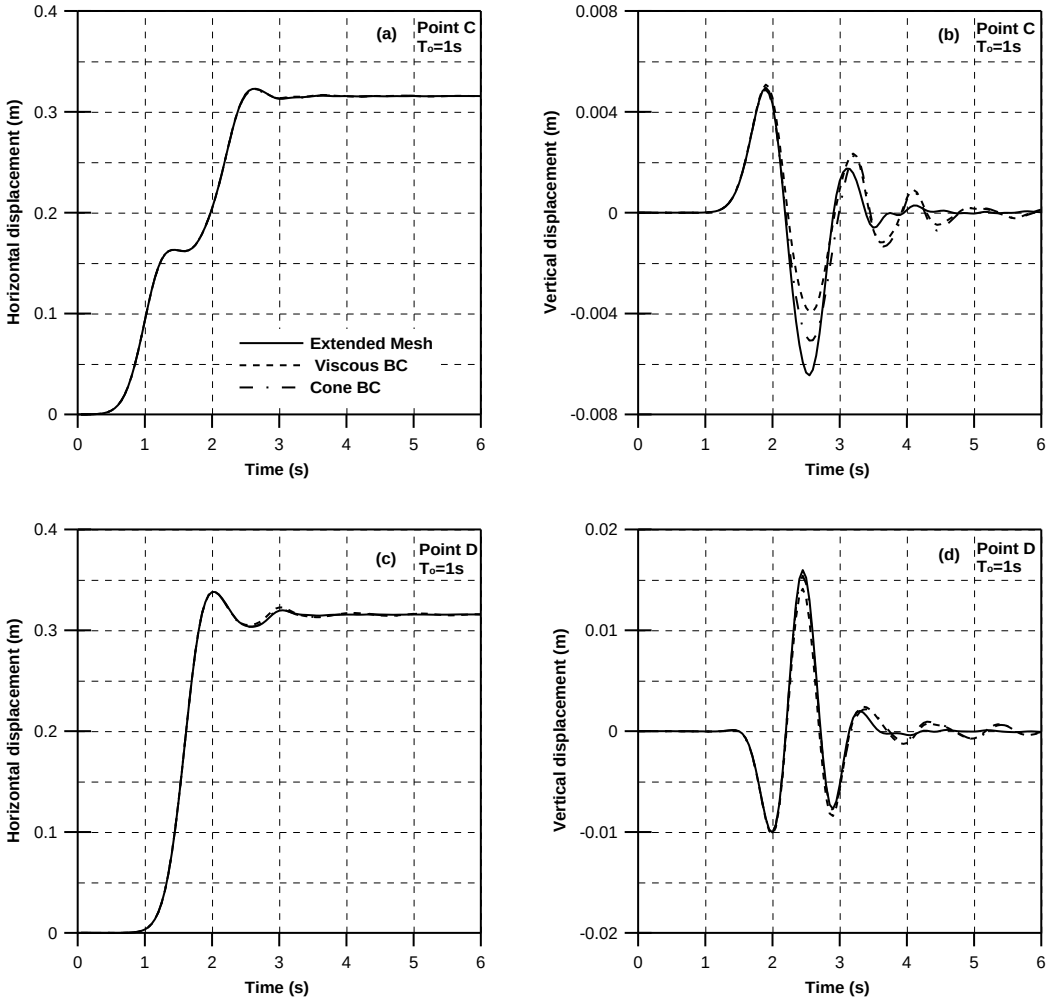

Figure 5: Comparison of the displacement response at nodes C, D for a pulse of T_o =1.0s

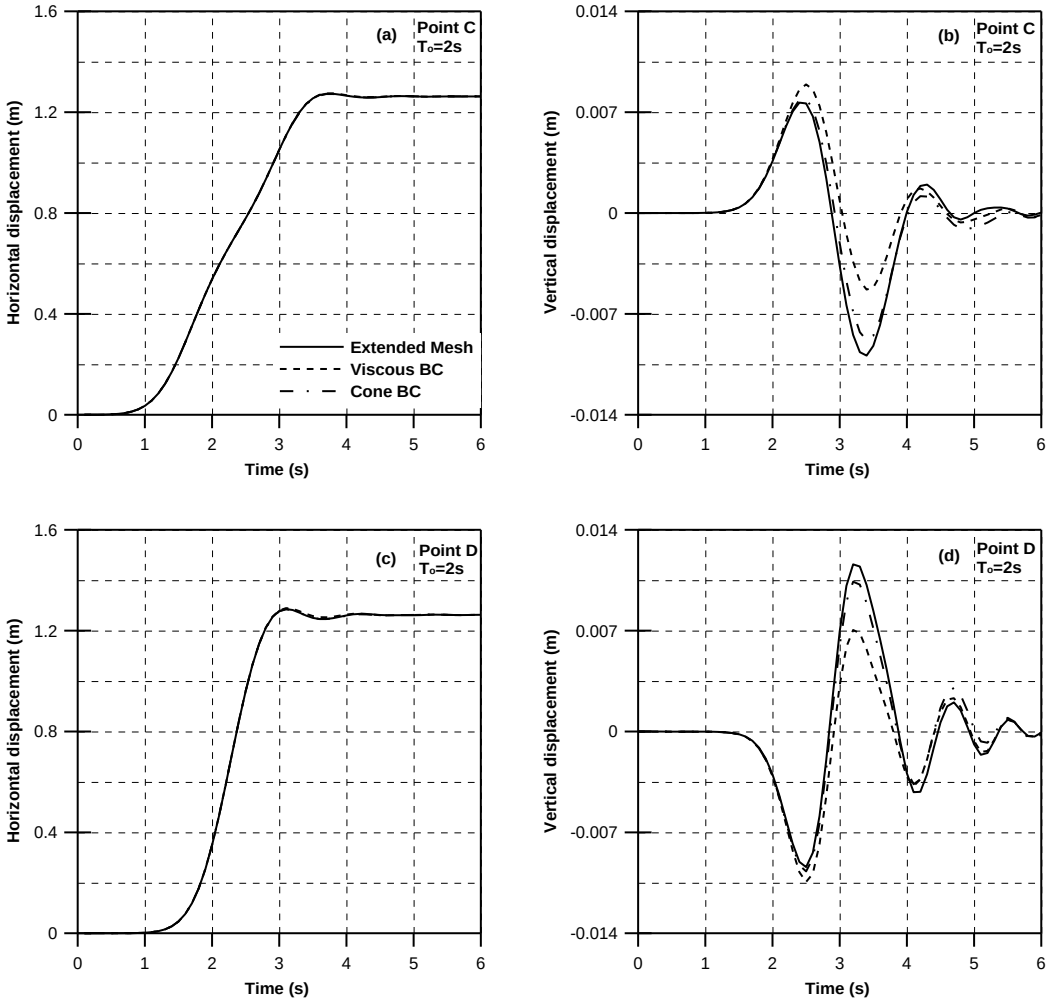

Figure 6: Comparison of the displacement response at nodes C, D for a pulse of T_o =2.0s

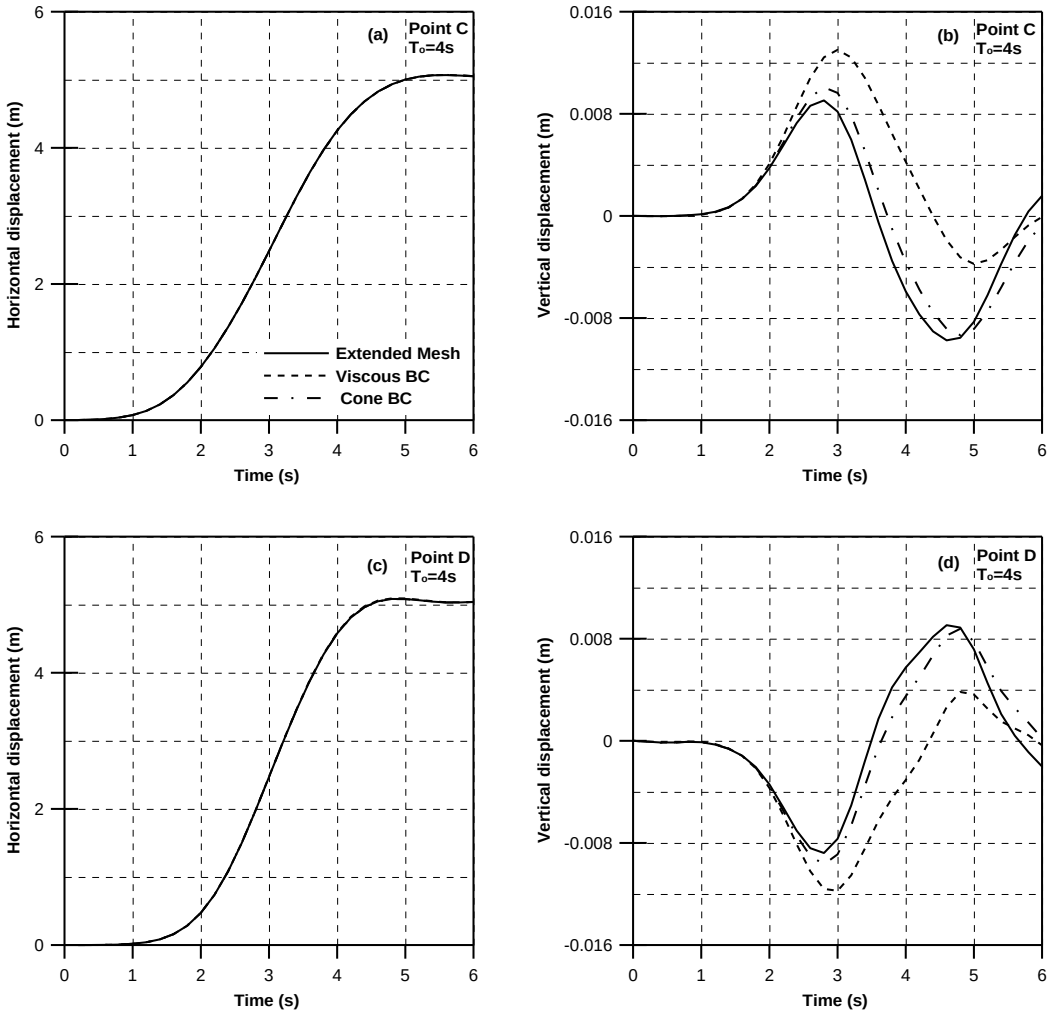

Figure 7: Comparison of the displacement response at nodes C, D for a pulse of T_o=4.0s

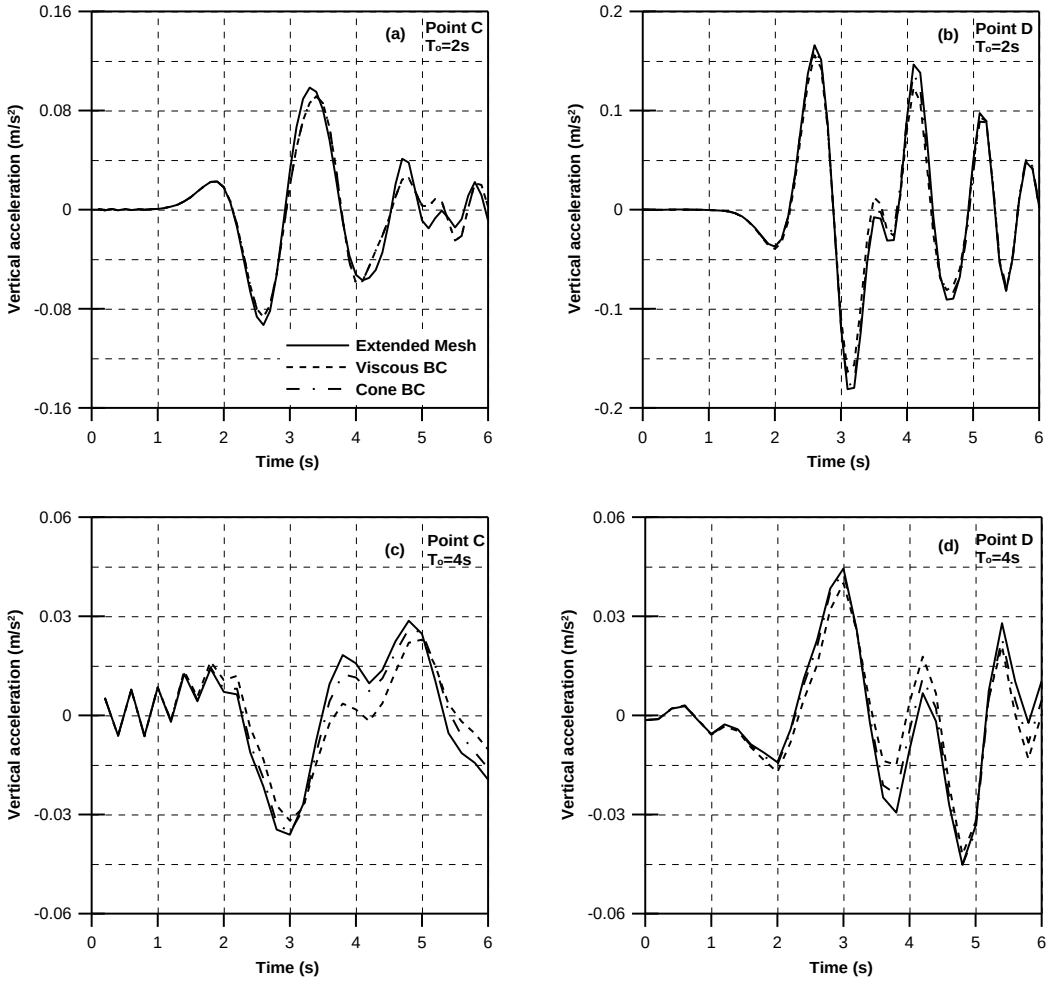

Figure 8: Comparison of the acceleration response at nodes C, D for pulses of T_o=2.0, 4.0s.

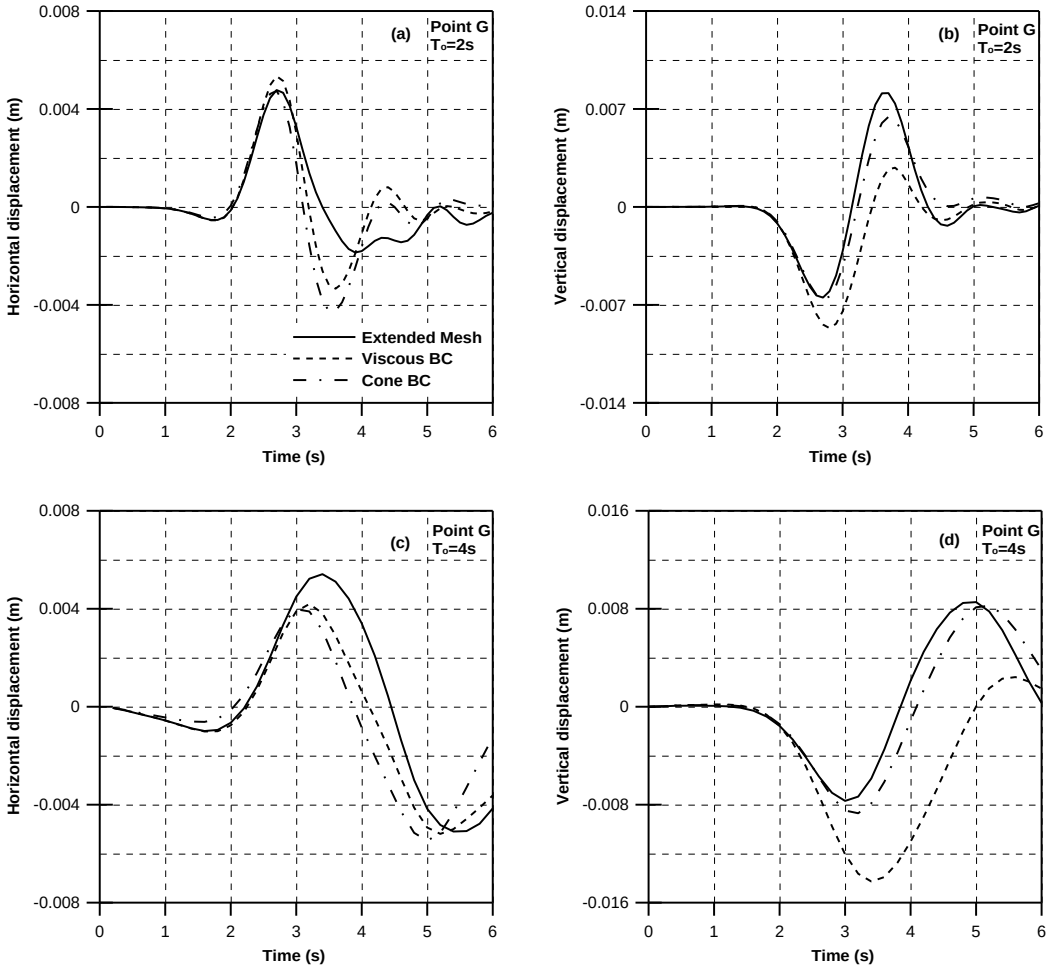

Figure 9: Comparison of the displacement response at node G for pulses of T_o=2.0s ,4.0s.

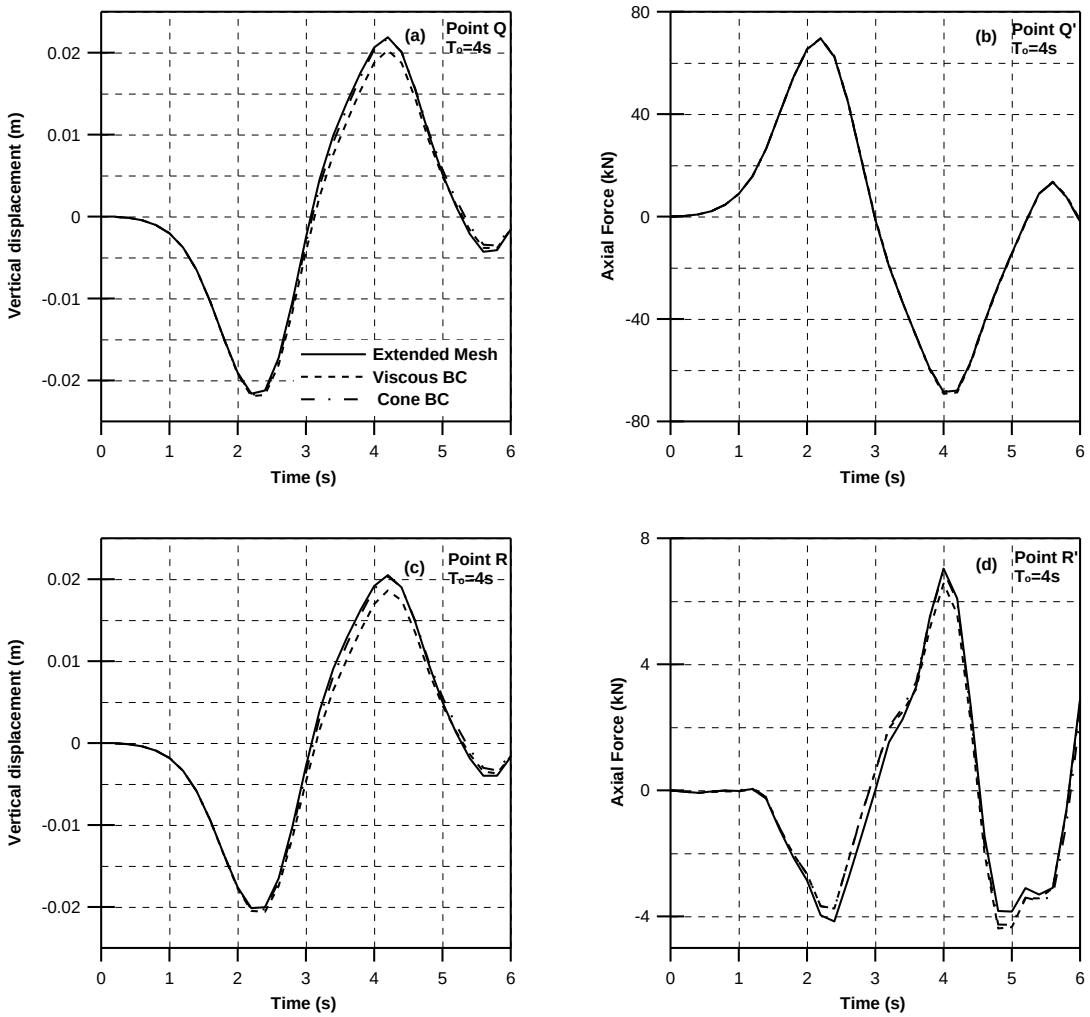

Figure 10: Comparison of vertical displacement and axial force time histories at nodes Q, R and integration points Q', R' respectively for T=4.0s.

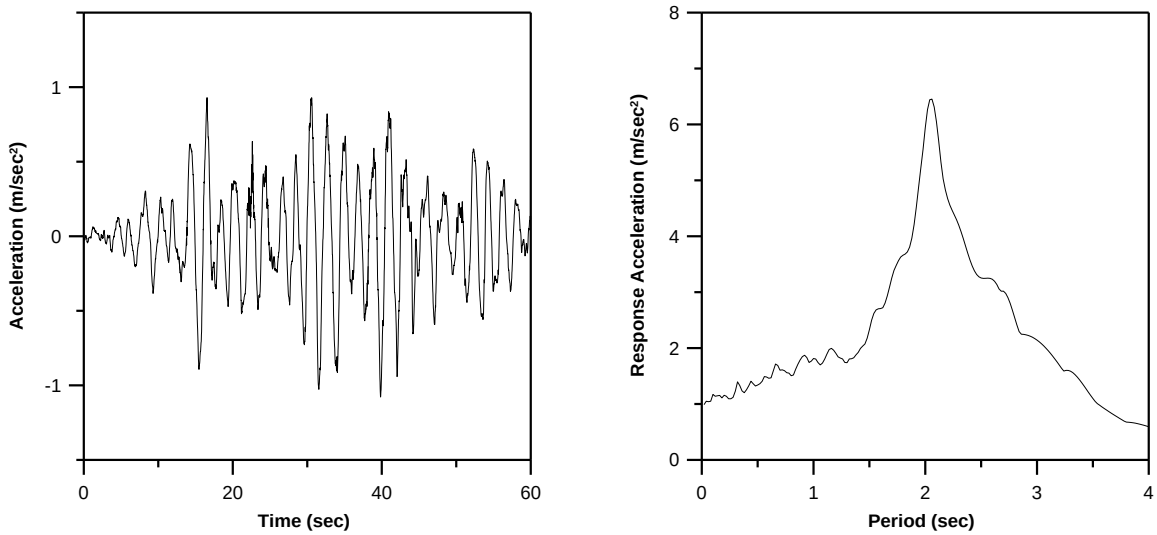

Figure 11: Filtered acceleration time history (a) and response acceleration spectrum (b) of the 1985 Mexico earthquake.

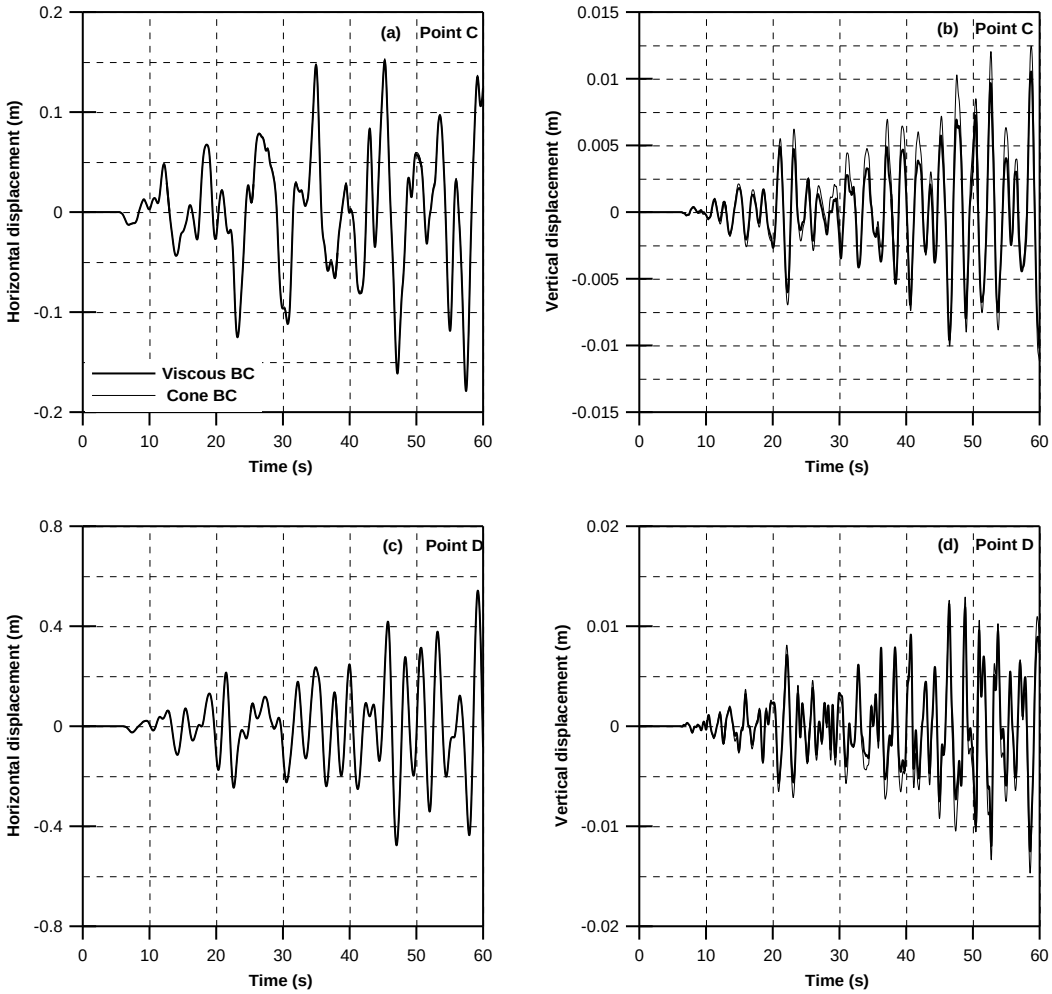

Figure 12: Comparison of the displacement response of nodes C, D

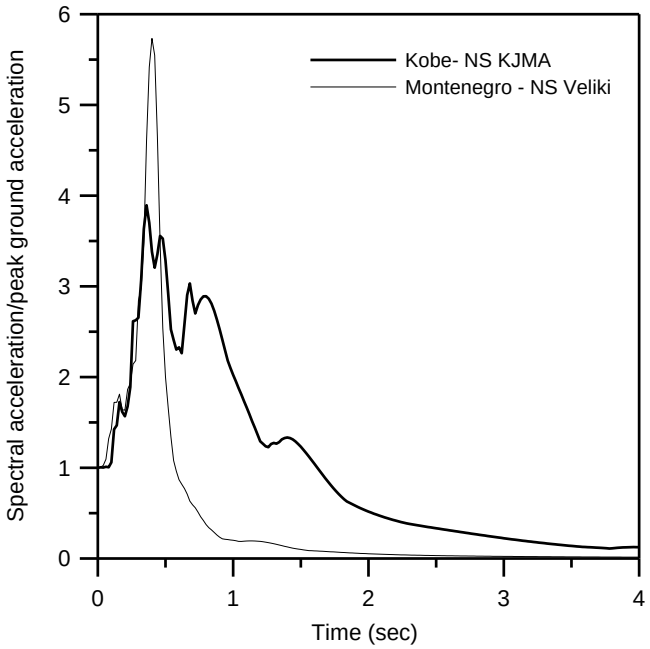

Figure 13: Normalised acceleration response spectra of KJMA and Veliki records

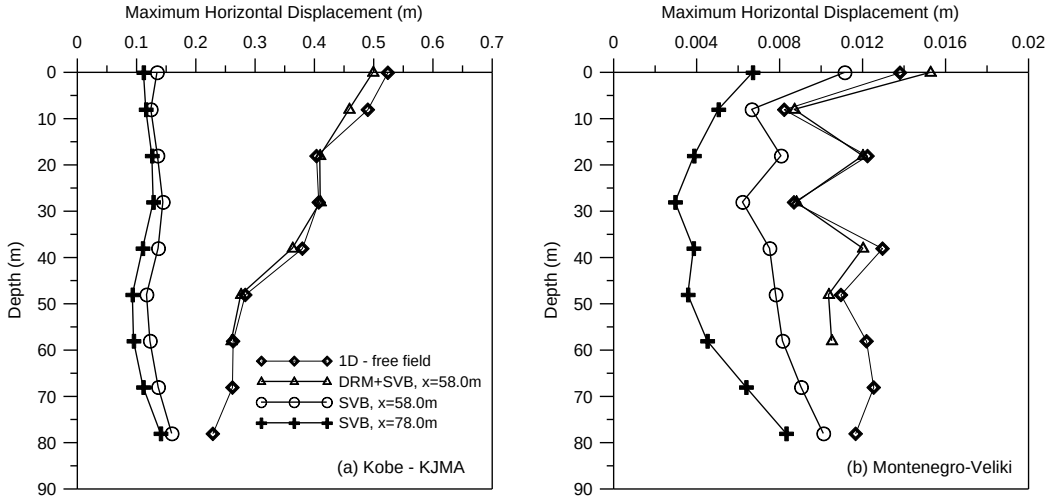

Figure 14: Maximum horizontal displacement profiles for (a) KJMA and (b) Veliki excitations computed with the 1D, DRM+SVB and SVB models

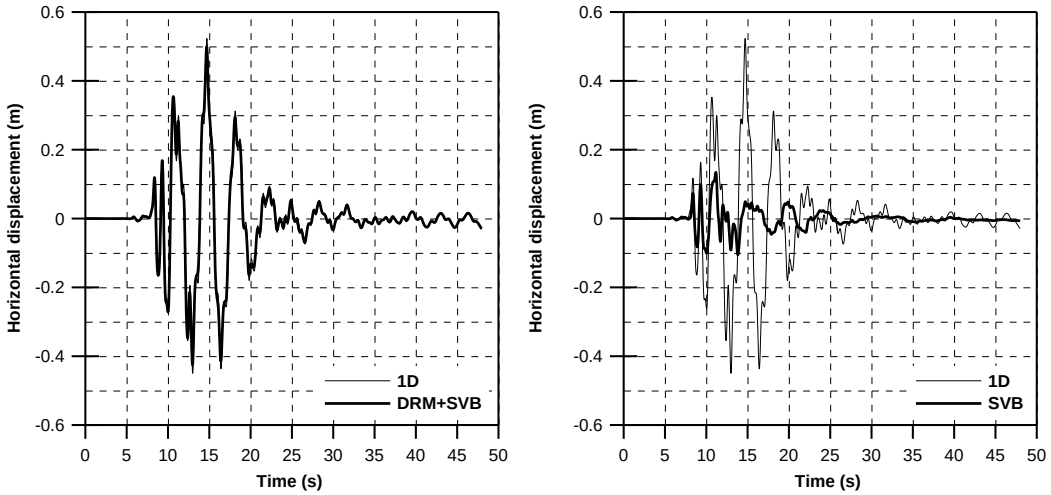

Figure 15: Comparison of the horizontal displacement time histories recorded at node T of the (a) DRM+SVB and (b) SVB models with the corresponding ones of the 1D model for the KJMA excitation.

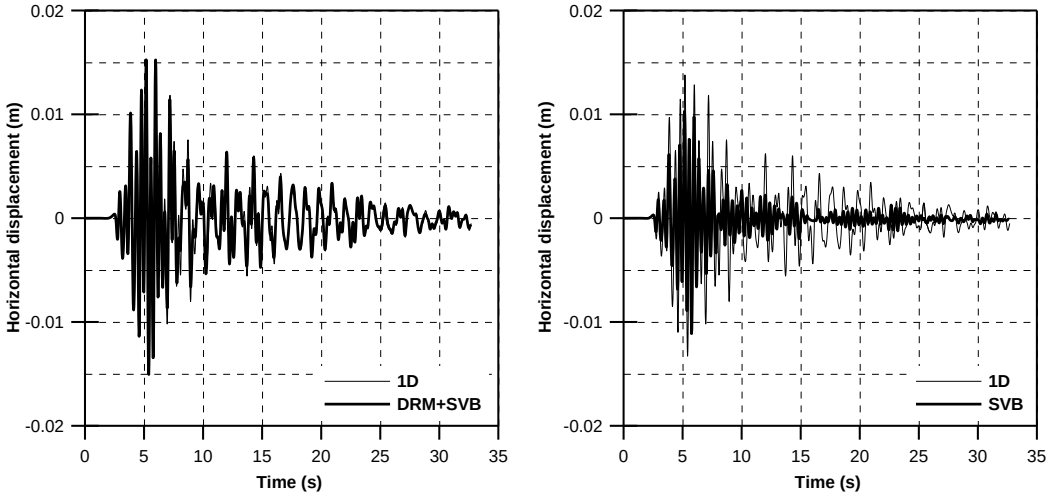

Figure 16: Comparison of the horizontal displacement time histories recorded at node T of the (a) DRM+SVB and (b) SVB models with the corresponding ones of the 1D model for the Veliki excitation.

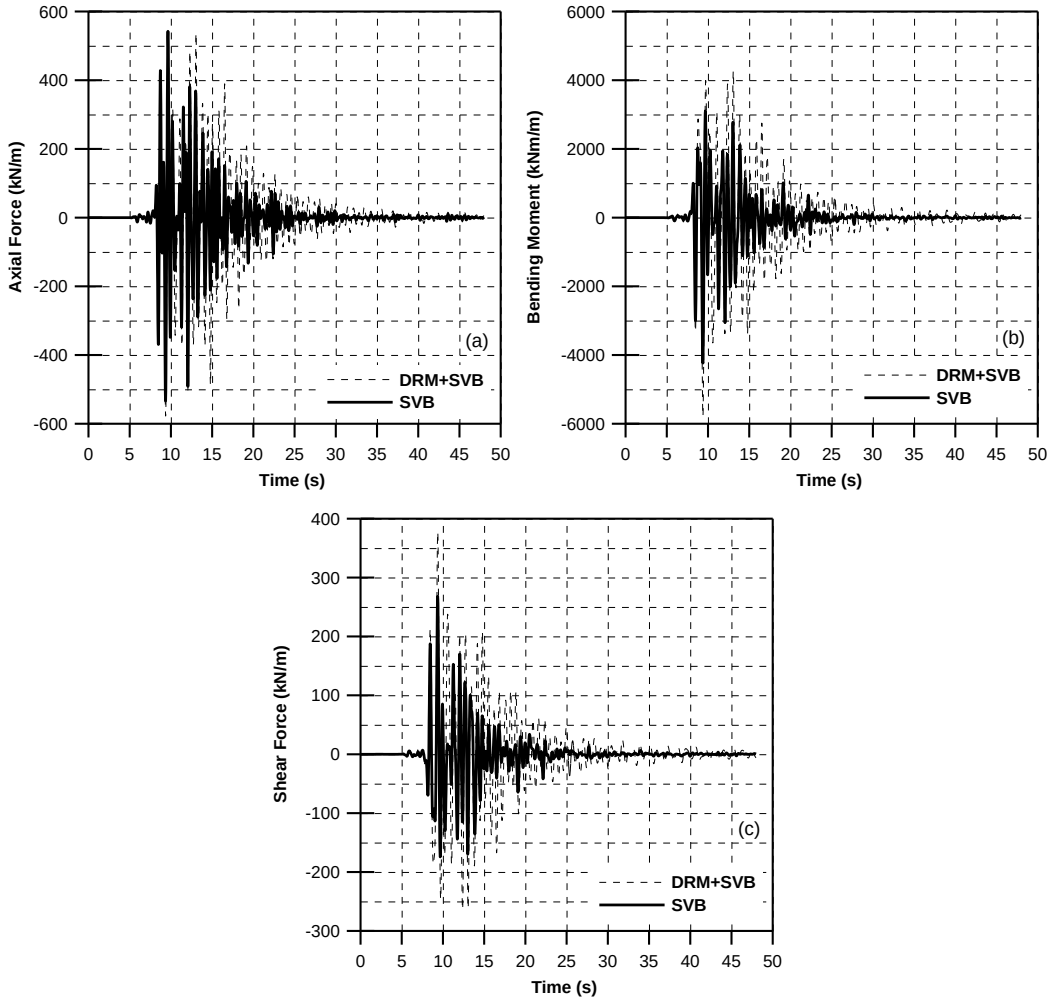

Figure 17: Time histories of (a) axial force, (b) bending moment and (c) shear force computed by the DRM+SVB and SVB model integration point Q' of the structure.

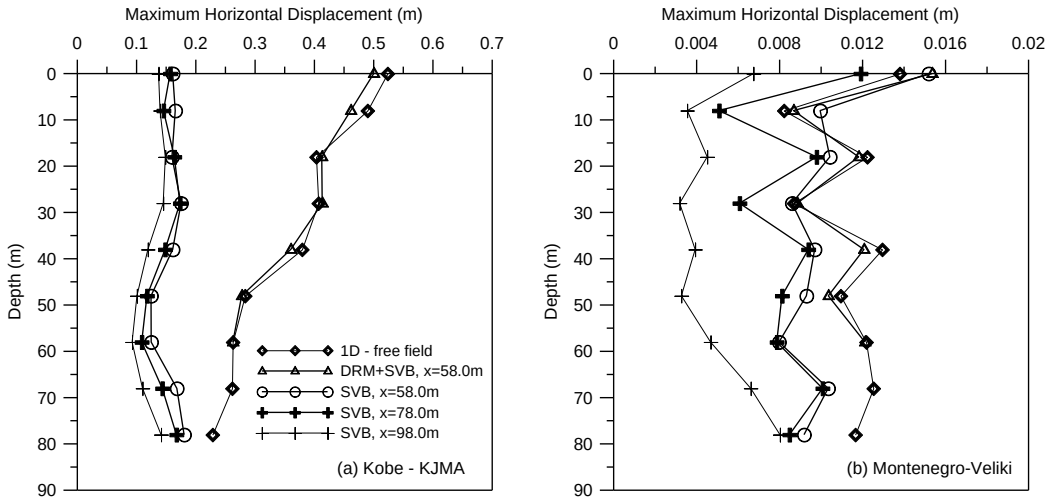

Figure 18: Maximum horizontal displacement profiles for (a) KJMA and (b) Veliki excitations computed with the 1D, DRM+SVB and SVB models using the 206x86 mesh.

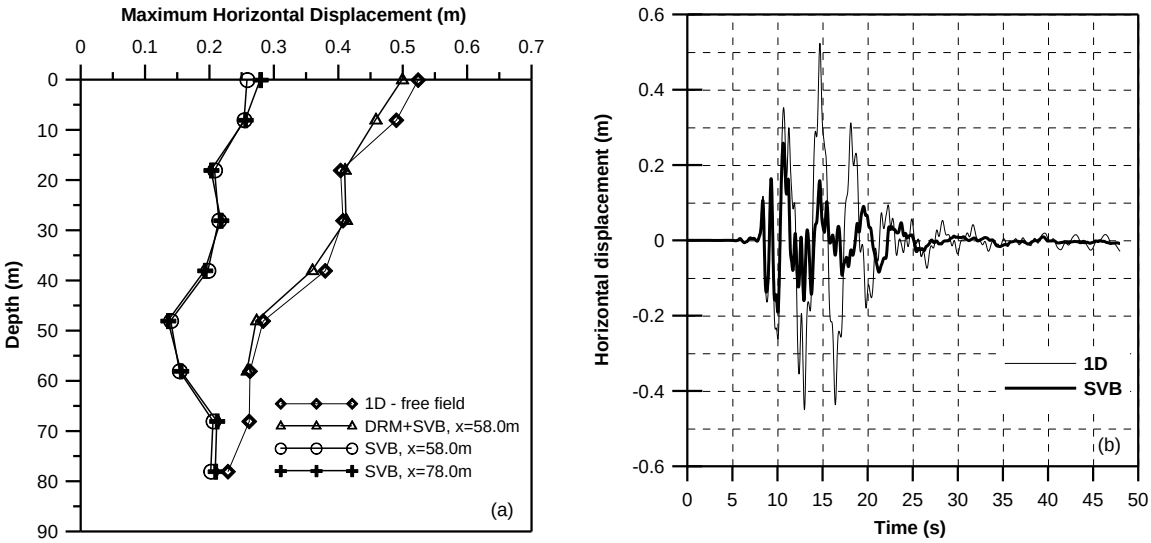

Figure 19: Maximum horizontal displacement profiles (a) and comparison of the horizontal displacement time history recorded at node T of the SVB model with the corresponding one of the 1D model for the KJMA excitation using the 300x86mesh (b).

9 Tables

Table 1: Material properties

	Soil	Concrete
E′ (kPa)	$50.0x10^3$	$30.0x10^6$
Vs (m/sec)	101.6	2170.0
ν′	0.25	0.2
γ (kN/m^3)	19.0	24.0
A	0.06496	0.06496
B	2.69E-3	2.69E-3

Table 2: Comparison of computational cost

		KJMA			VELIKI	
		Mesh 176x86m	Mesh 204x86m	Mesh 300x86m	Mesh 176x86m	Mesh 204x86m
Computational cost (min)	DRM+SVB	845	960	1213	576	655
	SVB	827	947	1204	566	640
Percentage difference between the DRM+SVB & SVB		2.2	1.4	0.8	1.8	2.3